

Circumgalactic medium of quasar host galaxies at $0.4 \leq z \leq 0.8$ probed by strong Mg II absorption

Paryag Sharma,^{1*} Raghunathan Srianand,² Hum Chand,¹ Labanya Kumar Guha³

¹Department of Physics and Astronomical Science, Central University of Himachal Pradesh, Dharamshala, 176215, India

²Inter-University Centre for Astronomy and Astrophysics, Post Bag 4, Ganeshkhind, Pune 411 007, India

³Indian Institute of Astrophysics, II Block, Koramangala, Bengaluru-560 034, India

Accepted XXX. Received YYY; in original form ZZZ

ABSTRACT

Using a sample of 166 projected quasar pairs we investigate the influence of active galactic nuclei on the circumgalactic medium (CGM) of the quasar host galaxies probed using strong Mg II absorption (i.e., $W_{2796} \geq 1\text{\AA}$) at impact parameters (D) < 100 kpc. The foreground quasars are restricted to the redshift range $0.4 \leq z \leq 0.8$ and have median bolometric luminosity and stellar mass of $10^{45.1} \text{erg s}^{-1}$ and $10^{10.89} M_{\odot}$ respectively. We report detections of Mg II absorption in 29 cases towards the background quasar and in 4 cases along the line of sight to the foreground quasars. We do not find any difference in the distribution of W_{2796} and covering fraction (f_c) as a function of D between quasar host galaxies and control sample of normal galaxies. These results are different from what has been reported in the literature, possibly because: (i) our sample is restricted to a narrow redshift range, (ii) comparative analysis is carried out after matching the galaxy parameters, (iii) we focus mainly on strong Mg II absorption and (iv) our sample lacks foreground quasars with high bolometric luminosity (i.e., $L_{bol} > 10^{45.5} \text{erg s}^{-1}$). Future studies probing luminous foreground quasars, preferably at lower impact parameters and higher equivalent width sensitivity is needed to consolidate our findings.

Key words: quasars: absorption lines – quasars: general – galaxies: haloes

1 INTRODUCTION

Since quasars were first discovered, their spectra revealed metal absorption lines produced by the intervening gas (Sandage 1965; Gunn & Peterson 1965; Burbidge et al. 1966; Burbidge 1967). Subsequent studies established that these metal absorbers were associated with foreground galaxies intersecting the quasar sightlines at low impact parameters (Bahcall & Salpeter 1966; Bahcall & Spitzer 1969; Opher 1974; Roeser 1975; Burbidge et al. 1977; Bahcall 1978; Sargent et al. 1982; Bergeron & Stasińska 1986; Steidel & Sargent 1992). This realization has led to the identification of an extended gaseous component surrounding galaxies. Various statistical properties of Mg II absorbers can be reproduced using this gaseous component, refer to as the circumgalactic medium (CGM), around galaxies (e.g., see, Petitjean & Bergeron 1990; Srianand & Khare 1994). The CGM also plays a crucial role in galaxy evolution, acting as a reservoir for gas that fuels star formation and accretion processes. Understanding the CGM's properties and its interaction with galactic components is essential for constructing a comprehensive picture of galaxy dynamics (Tumlinson et al. 2017; Fumagalli 2024).

Detecting diffused emission-lines allows direct spatial mapping of the gas and, in principle, provides an alternate probe of the CGM (Hennawi & Prochaska 2013; Martin et al. 2014; Cantalupo et al. 2014; Borisova et al. 2016; Farina et al. 2017; Arrigoni Battaia et al. 2018; Ginolfi et al. 2018; Drake et al. 2019; Cai et al. 2019; O'Sullivan et al. 2020; Guo et al. 2020; Burchett et al. 2021; Fossati

et al. 2021). However, such studies face significant challenges compared to absorption-line studies as the emission measure scales with the square of the gas density (n^2). Since the CGM typically has a low hydrogen number density ($n_H \sim 10^{-2} \text{cm}^{-3}$ or less), detecting such emission is inherently difficult. Additionally, the surface brightness of CGM emission is extremely faint relative to the sky and detector backgrounds, and surface brightness dimming increases steeply with redshift, further complicating detection.

In contrast, quasar absorption-line studies offer several advantages. The absorption-line detections are largely independent of redshift and the luminosity of the host galaxy and depends mainly on the signal to noise ratio (SNR) achieved for the quasar spectrum. Therefore, by choosing bright enough background sources high sensitivity can be achieved to detect even low column density gas. On the flip side, absorption-line studies provide only projected, pencil-beam measurements of gas surface density. In most cases, observations are limited to a single sightline per galaxy due to the rarity of suitably bright background quasars, making it difficult to fully characterize the spatial extent and morphology of the CGM. Therefore, one generally uses statistics based on a sample of quasar-galaxy pairs to characterize the average properties of CGM around galaxies. Quasar absorption-line studies have yielded profound insights into the nature of CGM (e.g., Nielsen et al. 2013; Mishra et al. 2018; Dutta et al. 2020, 2021, 2023; Joshi et al. 2024).

In this study we adopt the absorption-line technique to probe the CGM because the advent of large-scale spectroscopic surveys like the Sloan Digital Sky Survey (SDSS; Abdurro'uf et al. 2022) and the Dark Energy Spectroscopic Instrument (DESI; DESI Collabo-

* panditparyag@gmail.com

ration et al. 2024) has dramatically increased the number of known quasars, providing a significant sample in a narrow redshift range suitable for statistical analysis. In particular, we ask the question whether the properties of CGM, as probed by Mg II absorption, are same for normal galaxies and host galaxies of quasars (Bowen et al. 2006; Farina et al. 2014; Chen et al. 2023; Johnson et al. 2015). Since the samples used in previous studies span a wide range of redshifts and luminosities, comparisons to normal galaxies is not straight forward due to degeneracies inherent in such samples (e.g luminosity dependence vs. z -dependence if most of the high luminosity objects come from high redshifts). To enable a proper comparison between normal galaxies and galaxies hosting a quasar, a controlled investigation is needed, which serves as the main motivation for our work. To minimize the effects of redshift evolution in our study, we focus on quasar pairs where the foreground quasar falls within the redshift range $0.4 \leq z \leq 0.8$. The lower redshift limit of $z = 0.4$ ensures that Mg II absorption remains within the optical spectral range. Also we restrict the impact parameter to be less than 100 kpc which allows us to probe the inner regions of the CGM. Given the signal-to-noise limitations of large survey spectra, we concentrate our analysis on strong intervening Mg II absorbers.

This paper is organized as follows: Section 2 describes our sample and absorption line measurements. Section 3 presents our analysis and results, while Section 4 we present discussion and conclusion of our findings. Throughout this work, we assume a flat Λ CDM cosmology with $\Omega_m = 0.3$, $\Omega_\Lambda = 0.7$, and $h_0 = 0.7$.

2 SAMPLE AND ABSORPTION LINE MEASUREMENTS

The sample of projected quasar pairs used in this study is sourced from the Sixteenth Data Release of the Sloan Digital Sky Survey (DR16Q; Lyke et al. 2020), comprising of 7,50,414 quasars. We apply the following criteria to construct our sample:

- (i) We first demand that the transverse separation between quasar sight lines at the redshift of the foreground quasar is less than 100 kpc. This constraint is placed mainly to enable comparisons with CGM of the normal galaxy samples and is satisfied only by 1115 projected quasar pairs.
- (ii) We ensured that the Mg II absorption associated with the CGM of the foreground quasar is covered in the SDSS spectrum by restricting the redshift of the foreground quasar to be in the range $0.4 \leq z_f \leq 0.8$. This reduces the sample to 202 projected pairs.
- (iii) A minimum velocity offset of 6000 km s^{-1} is imposed between the redshifts of the foreground and background quasars to reduce the likelihood of quasar pairs being associated (as also used in previous study by Chen et al. 2023). This further reduces the size of our sample to 180 projected quasar pairs.
- (iv) To avoid contamination of the Mg II absorption by high- z Ly α forest in the background quasar spectra, we imposed the condition $(1+z_f) \times 2800 \geq (1+z_b) \times 1300$, where z_f and z_b are the redshifts of the foreground and background quasars respectively. After applying this conditions we are left with 149 projected quasar pairs.

One pair, featuring the foreground quasar J083649.46+484150.1 from Bowen et al. (2006), was also included in our sample. Additionally, we performed the same sample selection exercise on the DESI EDR (DESI Collaboration et al. 2024) and identified a total of 16 projected quasar pairs satisfying all the above constraints. Thus our final sample consists of 166 quasar pairs.

To start with we measure the 3σ upper limit of Mg II rest equivalent width (W_{2796}) in the spectrum of the background quasar within

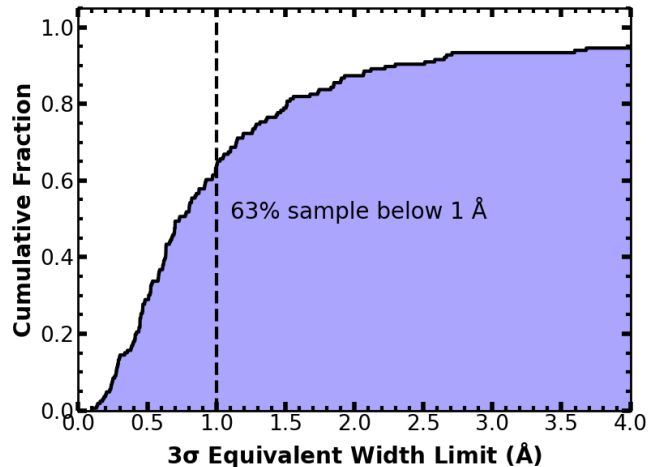


Figure 1. Cumulative distribution of the 3σ limit of W_{2796} in the spectrum of background quasars at the location of the foreground quasars. Vertical dashed line marks the rest equivalent limit of 1\AA .

$\pm 1500 \text{ km s}^{-1}$ with respect to the foreground quasar’s redshift, following the procedure described by Churchill et al. (2000). For this purpose, we have used line free regions after clipping the absorption lines, if present, in the above mentioned velocity range. Cumulative distribution of the 3σ limiting Mg II rest equivalent width for the full sample is shown in Figure 1. It is evident from the figure that only 63% (i.e., 105 sightlines) of the background quasar spectra have sufficient SNR so that we can detect Mg II absorption with $W_{2796} \geq 1\text{\AA}$ at $> 3\sigma$ level. For the statistical analysis of direct detections we use these projected quasar pairs and a limiting threshold W_{2796} of 1\AA .

Properties of Mg II absorption are known to depend on the bolometric luminosity (L_{bol}) of the foreground quasars (e.g., Johnson et al. 2015). We have used the bolometric luminosities for SDSS quasar pair from Wu & Shen (2022), and also used their method for estimation of L_{bol} of our the DESI quasars as well. In the top panel of Figure 2 we compare the bolometric luminosity of foreground quasars in our sample with those from Johnson et al. (2015). It is clearly evident that compared to their sample, quasars in our sample typically probe the low bolometric luminosity range. In particular while studying the luminosity dependent effects Johnson et al. (2015) defined the low luminosity objects as the ones with $\log L_{bol}(\text{erg s}^{-1}) < 45.5$ (marked with vertical dashed line in the Figure 2). As can be seen from the figure only 20 per cent of our quasars have L_{bol} in excess of $10^{45.5} \text{ erg s}^{-1}$. This is an important factor to remember while comparing our results with that of Johnson et al. (2015). In the bottom panel of Figure 2 we compare the distribution of L_{bol} between the two samples if we restrict ourselves to $D \leq 100 \text{ kpc}$ and foreground redshift range from 0.4 to 0.8. Clearly our sample provides a substantial improvement at low redshift and low bolometric luminosity range compare to the sample of Johnson et al. (2015).

We identify Mg II doublet features in the background quasar spectrum within $\pm 1500 \text{ km s}^{-1}$ of the foreground quasar redshift (as per the criteria in Chen et al. 2023) by visual inspection. These were confirmed when the Mg II doublet ratio is in the allowed range and by the presence of additional associated absorption from species such as Mg I and Fe II. We detected Mg II doublets along 29 background quasar lines of sight within $\pm 1500 \text{ km s}^{-1}$ from z_f . Out of these 29 detections, 18 detections have their measured Mg II rest equivalent widths significant at $> 3\sigma$ level and in the remaining cases the mea-

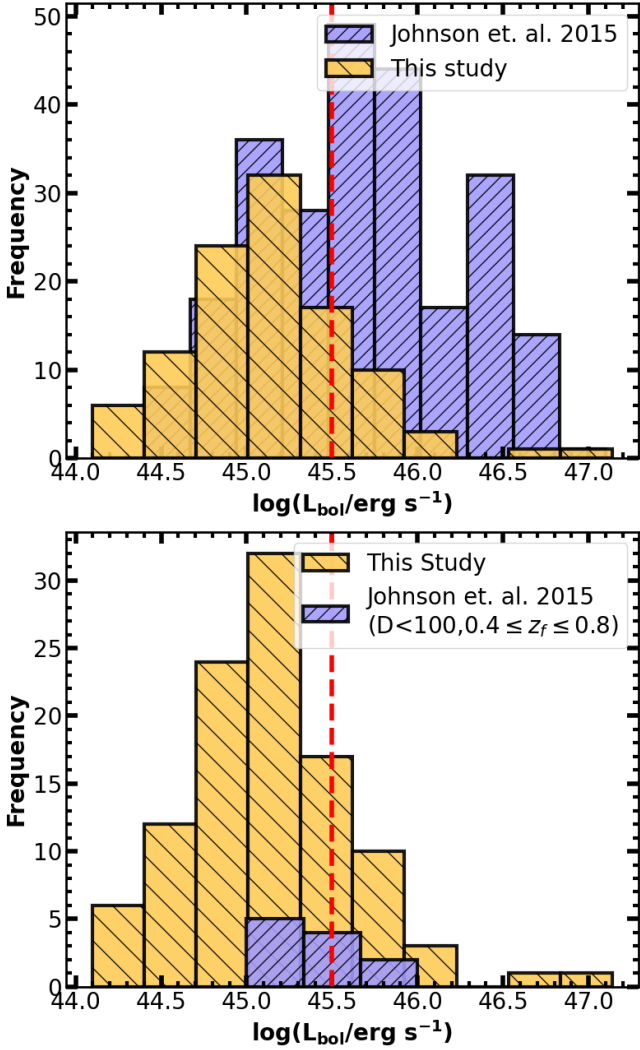


Figure 2. Comparison of the bolometric luminosity of quasars in our sample with those in the sample of Johnson et al. (2015). *Top Panel:* Shows the comparison with their full sample. *Bottom Panel:* Focuses on quasars within the same redshift and impact parameter ranges considered in our study. The vertical dashed line marks $\log(L_{\text{bol}}/\text{erg s}^{-1}) = 45.5$, the division between the luminous and low luminosity quasars used by Johnson et al. (2015).

sured equivalent widths are at $\sim 2\sigma - 3\sigma$ level. In Table 1 we provide the details of the project quasar pairs, impact parameter (D) at the redshift of the foreground quasar, Mg II rest equivalent width or its 3σ upper limit in case of non-detections and absorption redshift. For completeness, we also examined quasar pairs with a velocity separation of less than 6000 km s^{-1} . Among 22 such pairs, we detected Mg II absorption in 3 cases. However, these pairs are excluded from our analysis, as the absorption could originate either from the CGM of the foreground quasar or from the associated absorption of the background quasar. We also searched for Mg II absorption in the spectra of foreground quasars within a 3000 km s^{-1} window blueward of their redshift to identify any line-of-sight absorption. Mg II absorption is detected in only four out of 166 cases.

Publicly available systemic redshifts of SDSS quasars are known to exhibit systematic biases of $\Delta z/(1+z) \geq 0.002$ (i.e., $\geq 600 \text{ km s}^{-1}$). Hewett & Wild (2010) have improved the accuracy by a factor ~ 20 using Ca II absorption from the host galaxy and low ionization emission lines. In the SDSS DR16 catalog, revised redshifts are provided

for quasars where systematic corrections were applied; however, in some cases, only visually inspected redshifts are reported, which are less reliable. To ensure consistency and accuracy, we adopted the improved systematic redshifts for foreground quasars provided in Wu & Shen (2022). To obtain accurate absorption redshifts, we utilized VoigtFit (Krogager 2018) to simultaneously fit the Mg II 2796, 2803 and Fe II 2600 absorption lines. In cases where the signal-to-noise ratio (SNR) was low and simultaneous fitting was not feasible, we fitted only the Mg II lines, selecting one or both depending on the line profiles. To compare the properties of Mg II absorption from the quasar host galaxies in our sample and normal galaxies at $0.4 \leq z \leq 0.8$, we use the data from Nielsen et al. (2013, refer to as MAGICAT sample) and Huang et al. (2021) for normal galaxies and refer to them collectively as "galaxy sample".

In Figure 3, the top panel illustrates the velocity offsets of the detected absorbers relative to the foreground quasar. The bottom panel of Figure 3 presents the velocity offset distribution for the galaxy sample within the selected redshift and impact parameter ranges. We performed a KS test between distribution of velocity offset between two samples. The initial analysis yielded a KS statistic of 0.44 with a corresponding p_{null} of 0.002, suggesting a statistically significant difference between the two distributions. However, it is important to consider the potential impact of the quasar's inherent velocity offset, calculated as $\mu = 65.68 \text{ km s}^{-1}$, which may originate from systematic uncertainties in obtaining systemic redshift of the foreground quasars. After accounting for this offset, a subsequent KS test returned a statistic of 0.186 with a p_{null} of 0.528. This result indicates that, when corrected for the possible quasar's velocity offset, there is no significant difference between the velocity offset distributions for the two sample considered here.

3 RESULTS

In this section we summarize our results of comparing properties of Mg II absorption originating from quasar host galaxies and normal galaxies at $0.4 \leq z \leq 0.8$ and at impact parameters $D \leq 100 \text{ kpc}$.

3.1 Equivalent width vs. Impact parameter

The rest equivalent width of Mg II absorption is known to show clear anti-correlation with the impact parameter (Bergeron & Boissé 1991) albeit with a large scatter (Chen et al. 2010; Nielsen et al. 2013). This relationship is usually approximated by the log-linear relationship as,

$$\log W_{2796}(\text{\AA}) = \alpha \times D (\text{kpc}) + \beta \quad (1)$$

where β is $\log W_{2796}(\text{\AA})$ at $D = 0 \text{ kpc}$ and α provides the exponential scale length. In Figure 4 upper panel we compare the correlation between W_{2796} and D for our sample with that of the galaxy sample chosen over the same redshift range considering only detections. The best fit relationship is shown in solid and dashed lines respectively for our sample and the galaxy sample. Best fitted values of α and β are provided in Table 2. For obtaining this we have used the standard procedure as detailed in Guha et al. (2022). It is evident that the best fitted α values are nearly same for both samples. However β value obtained for our sample is higher than that obtained for the galaxy sample. But, the difference is not statistically significant (i.e., only at $\sim 1.3 \sigma$ level) due to large errors.

In bottom panel of Figure 4, we repeated the analysis by including upper limits. In this approach, the integral for the likelihood of non-detections is evaluated with a lower bound of $W_{2796} = 0 \text{\AA}$. Fit results

No.	Background Quasar	Redshift z_b	Foreground Quasar	Redshift z_f	D_{\perp} (kpc) at z_f	z_{abs}	W_{2796} (Å) Mg II 2796	$Err W_{2796}$ (Å) Mg II 2796
1	J003715.09+055029.2	2.096	J003715.29+055022.7	0.517	44.155	0.517	0.72	0.35
2	J012906.68+004322.9	1.838	J012906.33+004322.0	0.743	38.928	0.742	2.43	1.03
3	J013416.95+330854.5	1.136	J013416.69+330855.9	0.706	25.514	–	0.39	-1
⋮	⋮	⋮	⋮	⋮	⋮	⋮	⋮	⋮

Table 1. Table displaying the information about our quasar pair sample. The cases in which there is a detection of Mg II absorption line at the foreground redshift have the equivalent width specified. For cases where the line has not been detected, we provide the 3σ W_{2796} threshold and the error associated with it -1. The entire table consisting of 166 quasar pairs is available online; here we display its structure and contents.

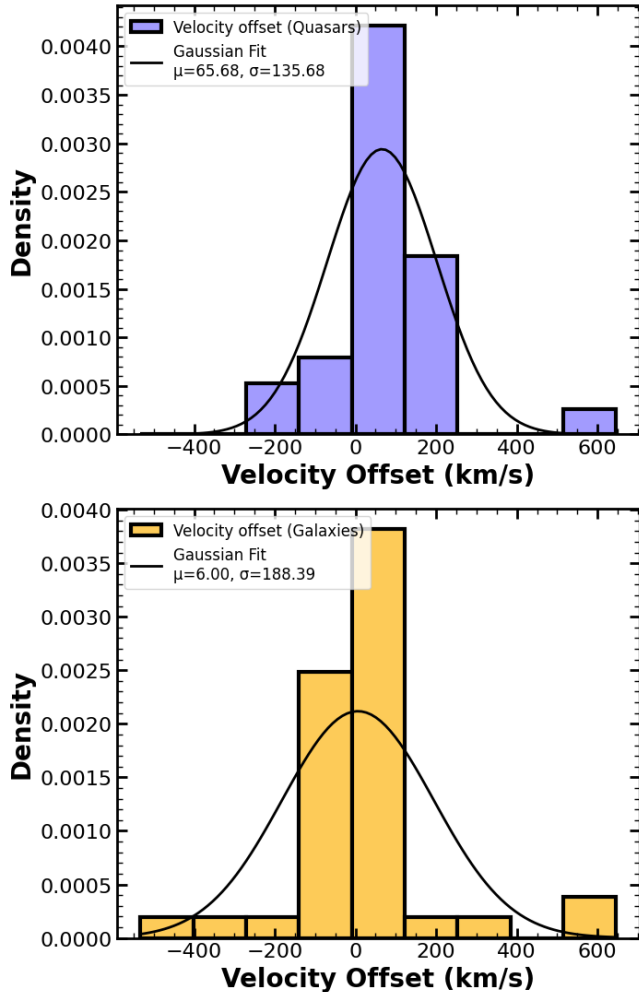


Figure 3. *Top panel:* Displays the velocity offset between the redshift of the foreground quasar and the Mg II absorption redshift, highlighting a strong correlation between the two except mean offset quasar reading. *Bottom panel:* Illustrates the same velocity offset for galaxies with $D < 100$ and $0.4 \leq z \leq 0.8$, providing further context for the observed trends.

are presented in Table 2. Recalling that in our sample we considered only sightlines that have sensitivity to detect the Mg II line with rest equivalent width greater than 1\AA . Clearly inclusion of upper limits in our analysis makes the two distributions statistically similar (i.e., both α and β measurements are well within 1σ). Also, the α values obtained with and without including the upper limits are nearly same. The β values obtained for galaxies are also not very different based on whether we include the upper limits or not. This is because in this sample there are lot more detections compare to upper limits. On the

Table 2. Comparison of α and β values for Mg II W_{2796} vs. D relation (e.g., see Figure 4)

Sample ($0.4 \leq z \leq 0.8$)	α	β	σ
Considering only detections			
Quasar	-0.008 ± 0.002	0.430 ± 0.110	0.455 ± 0.083
Galaxies	-0.009 ± 0.002	0.297 ± 0.041	0.737 ± 0.088
Considering detections & limits			
Quasar	-0.010 ± 0.001	0.295 ± 0.039	0.346 ± 0.034
Galaxies	-0.011 ± 0.002	0.315 ± 0.052	0.691 ± 0.075

other hand we see the β value decreases slightly when we include the upper limits in the case of quasar sample.

As discussed in Guha et al. (2024) the relationship between W_{2796} and impact parameter (D) is sensitive to the distribution of impact parameter probed. For example, inclusion of Ultra-Strong Mg II absorbers (USMgII) and Galaxy On Top of Quasars (GOTOQs) that probe typical impact parameters ≤ 30 kpc makes β values increase by a factor of 1.7 compared to the literature data that usually probe larger impact parameters (see Guha et al. 2022; Guha & Srianand 2023; Guha et al. 2024; Guha & Srianand 2024). Note both our quasar and galaxy samples used here have very few sightlines at $D < 20$ kpc. This could explain why our β values are less than the best fit values obtained by Guha et al. (2024).

Further, we note that the distribution of the impact parameter D in our quasar sample differs significantly from that of the galaxy sample ($p_{null} = 0$), primarily because the quasar sample includes a larger number of data points at higher impact parameters. To investigate whether this discrepancy biases our results, we resampled the quasar data based on the impact parameter distribution of the galaxy sample, ensuring an equal number of points in each subset. This resampling was performed multiple times. In Figure 5, we plot the distributions of α and β obtained from these resampled quasar datasets and compare them with the corresponding fit for the galaxy sample (including upper limits) within our redshift range. The medians of the Gaussian fits are found to be approximately equal to the values of α and β obtained for the galaxy sample within measurement uncertainties. This indicates that the similarity observed in the W_{2796} vs. D relation between the galaxy and quasar samples is not biased by the differences in their impact parameter distributions.

It was also suggested that at a given impact parameter the measured W_{2796} might depend on the galaxy luminosity (see discussions presented in, Guha et al. 2024). Therefore, next we explore whether such a trend is present with respect to the bolometric luminosity of quasars. We also searched for a possible correlation between $\log(W_{2796}) - \alpha \times \log(D)$ and L_{bol} . We did not find any significant correlation between the two quantities (Spearman Rank correlation: -0.037 , p_{null} : 0.704). This implies that the scatter in W_{2796} vs. D plot is not driven by the dependence of this relationship on L_{bol} , at least in the sample considered here. This nominally

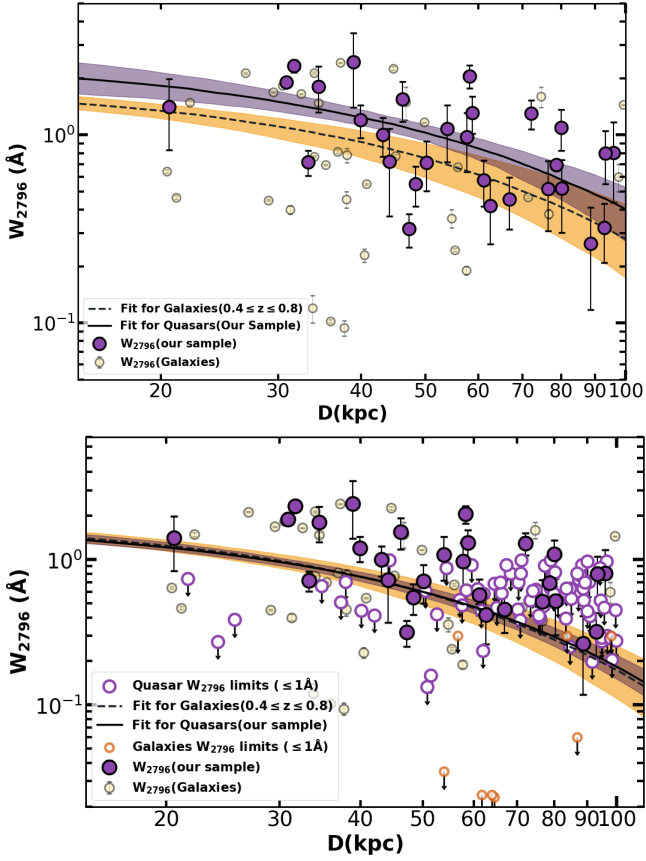


Figure 4. *Top panel:* The relationship between W_{2796} and the impact parameter (D) for foreground quasars. Violet filled circles represent cases with detected Mg II absorption. The faded yellow-filled circles are detections for galaxies. The solid black line and the violet shaded region around it indicate the fit for quasars, while the black dashed line and the yellow shaded region around it show the fit for the galaxy sample over the redshift range $0.4 \leq z \leq 0.8$. *Bottom Panel:* Same plot as the top panel with upper limits included.

contradicts Chen et al. (2023), possibly due to the higher luminosity (with median $\log L_{\text{bol}}/\text{erg s}^{-1} = 45.66$) of their stacked sample.

3.2 Mg II covering fraction (f_c)

The covering fraction is defined as the ratio of number of detections above a threshold rest equivalent width and total number of lines of sight probed having the required sensitivity to detect Mg II absorption above the chosen threshold. In Figure 6, we present the covering fractions of Mg II absorbers for three different threshold W_{2796} in two impact parameter bins having equal number of sightlines. First, we observe that our sample follows the well-established trend of decreasing covering fraction with increasing impact parameter and rest equivalent width threshold. For comparison we show the results obtained for MAGICAT galaxies Nielsen et al. (2013) and results obtained by Chen et al. (2023) for their full sample of galaxies. Our covering fraction measurements are consistent with the literature values. However, to draw a firm conclusion it is necessary to restrict the galaxy sample to the same redshift and impact parameter range as the quasar sample.

To achieve this, as before, we resample the quasar data to match the impact parameter distribution of the galaxy sample. We then calculate the average covering fraction within $D = 100 \text{ kpc}$. This

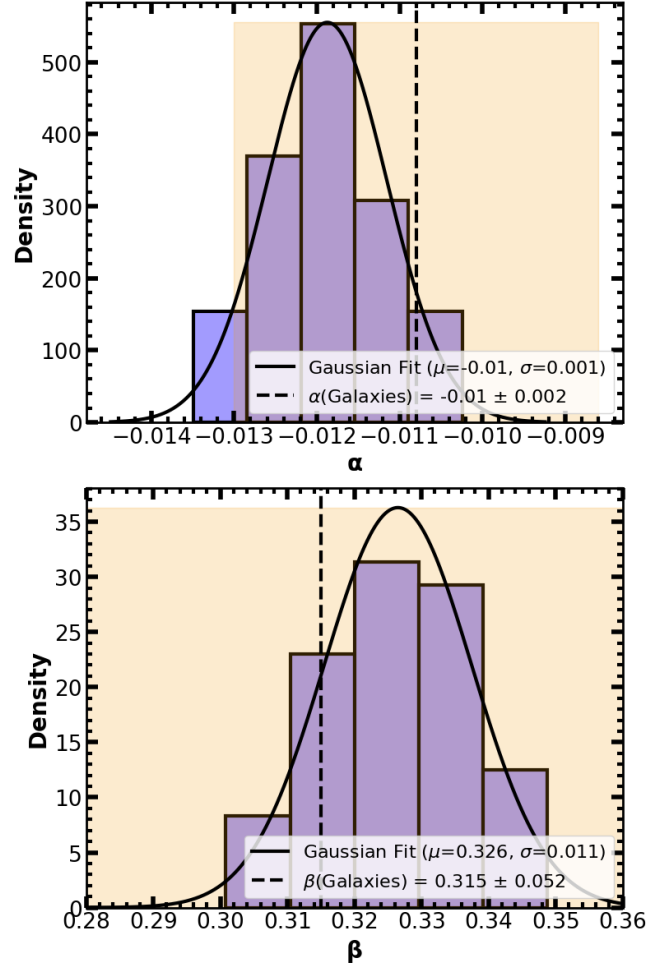


Figure 5. Figure shows the distributions of α (top panel) and β (bottom panel) for various realizations of control sample of quasars matching in impact parameter of galaxy data with impact parameter tolerance of 10 kpc. The results indicate that both distributions are consistent with each other, suggesting no significant discrepancies in the parameter values despite the imposed selection criteria. The vertical dashed lines represent the α and β values for the galaxy sample, while the shaded region indicates the associated error.

process is repeated multiple times to generate a distribution of covering fractions. The resulting covering fraction distribution for quasars is presented in Figure 7, along with the covering fraction for normal galaxies, represented by a vertical black dashed line. The shaded region around this line indicates the corresponding uncertainty. As evident from the figure, the covering fraction for quasar host galaxies remains well within the 1σ uncertainty of the covering fraction observed for normal galaxies.

Johnson et al. (2015) found a strong correlation between the covering fraction and bolometric luminosity. They also observed that the covering fraction measured at a given impact parameter is higher for quasar host galaxies with high luminosities ($\log L_{\text{bol}}/\text{erg s}^{-1} > 45.5$) compared to normal galaxies. To explore this, in Figure 8, we plot W_{2796} as a function of L_{bol} where we have also included 3σ limits for $W_{2796} \geq 1\text{Å}$. No significant correlation is evident between these two quantities, as indicated by the Spearman rank correlation coefficient of -0.036 with a p_{null} of 0.71. Next, we divide the sample into two luminosity at $\log L_{\text{bol}}/\text{erg s}^{-1} = 45$. The estimated covering fractions for absorbers with $W_{2796} \geq 1\text{Å}$ are also shown

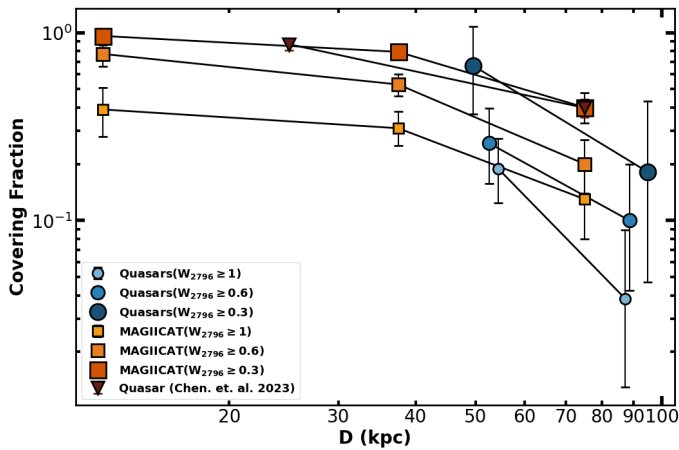


Figure 6. Comparison for the covering fraction of the CGM of galaxies hosting quasar in our sample with that of (i) similar study (i.e., quasar hosting galaxies) by [Chen et al. \(2023\)](#) and (ii) the CGM study of normal galaxies in MAGIICAT by [Nielsen et al. \(2013\)](#).

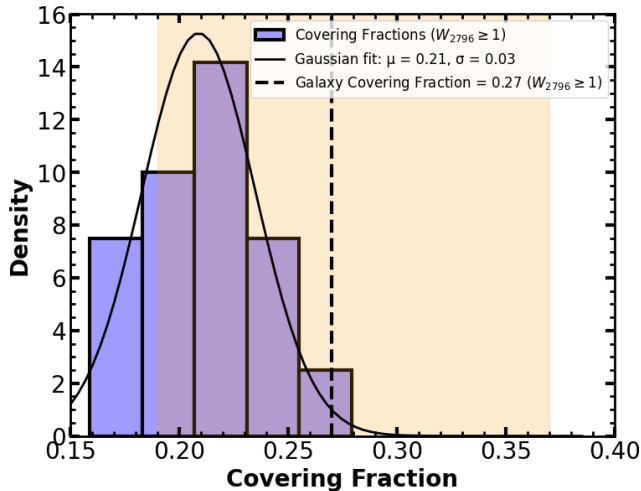


Figure 7. Comparison of the covering fraction distribution of quasars with galaxies, selecting quasars with impact parameters within a matching tolerance of 10 kpc for the galaxy sample, constrained by $D < 100$ kpc and foreground galaxies with redshifts in the range $0.4 \leq z \leq 0.8$. The vertical dashed line shows the covering fraction and the associated error for the galaxy sample with the same range of redshift and impact parameter.

in Figure 8. We observe a clear increasing trend in covering fraction with increasing L_{bol} . Since we consider a restricted range of impact parameters and redshifts, the redshift distributions of the two luminosity bins are consistent with each other, as confirmed by a KS test yielding a p_{null} of 0.45. Similarly, the KS test for the impact parameter distributions results in a p_{null} of 0.33, indicating no significant difference between the two luminosity samples which can create a bias in the calculation of the covering fraction. Thus, we confirm a weak dependence of the covering fraction on bolometric luminosity. However, we do not find the measured covering fraction for any of the two bins being statistically different from that measured for the galaxy sample.

In Figure 8, we also include the covering fraction measured for the sample of [Johnson et al. \(2015\)](#) for $D < 100$ but without any restriction on the redshift range. Their measured average luminosity (see

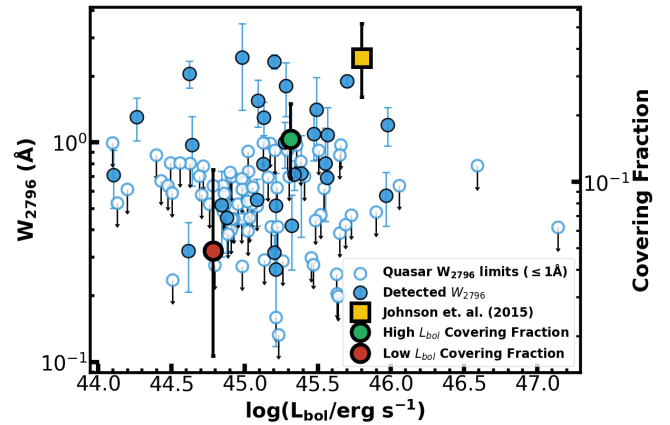


Figure 8. The figure illustrates the variation of W_{2796} with bolometric luminosity for the quasar sample. Overlaid in the right hand side ordinate are the covering fractions for two luminosity bins and $W_{2796} \geq 1$.

Figure 2) and covering fraction (i.e., $0.36^{+0.15}_{-0.12}$) are higher than those obtained for our sample ($0.11^{+0.04}_{-0.03}$). This once again indicates the increase in covering fraction with increasing bolometric luminosity. Note, the sample of [Johnson et al. \(2015\)](#) covers a wider redshift range and any dependence of f_c on z could affect our interpretation of this result. Also the covering fraction for the galaxy population (i.e. $0.27^{+0.10}_{-0.08}$) is not significantly different than what is obtained for the sample of [Johnson et al. \(2015\)](#). Thus our study indicates the need for a detailed investigation of these issues with larger samples well matched in luminosity, impact parameter and redshift distribution between normal galaxies and quasar host galaxies.

3.3 Influence of stellar mass

It is well documented in the literature that W_{2796} vs. D as well as f_c vs. D relationships depend on the stellar mass of the galaxy (see for example, [Lan 2020](#)). So it is important to check how the stellar mass distribution of quasar host galaxies and normal galaxies used in this work compare with each other. In Figure 9, we plot stellar mass vs. impact parameter for both the sample. This figure also compares the histogram distribution of stellar masses for both the samples. For the galaxy sample, we calculated galaxy stellar masses only for cases where photometry was available in SDSS DR17 ([Abdurro'uf et al. 2022](#)) or DECaLS ([Decarli et al. 2010](#)) using the method described in [Guha et al. \(2022\)](#). For quasars, the stellar mass was estimated using the empirical relation between black hole mass and host galaxy stellar mass from [Decarli et al. \(2010\)](#):

$$\log \frac{M_{\text{BH}}}{M_{\text{host}}} = (0.28 \pm 0.06) z - (2.91 \pm 0.06). \quad (2)$$

Here, M_{host} represents the stellar mass, while M_{BH} denotes the black hole mass. For SDSS quasars, M_{BH} values were obtained from the catalog of [Wu & Shen \(2022\)](#). For quasars from the DESI EDR, we applied the same methodology as described in their work to derive M_{BH} , ensuring consistency in stellar mass estimation. As can be seen from the Figure 9 that the stellar mass distributions are nearly same. The median stellar mass for the quasar sample is found to be $10^{10.89} M_{\odot}$, whereas for the galaxy sample, it is $10^{10.86} M_{\odot}$. To statistically compare these distributions, we performed KS test, which resulted in a KS statistic of 0.170 and a p_{null} of 0.341. Given the high p_{null} , we conclude that there is no significant difference between the two distributions. This result indicates that quasars in our

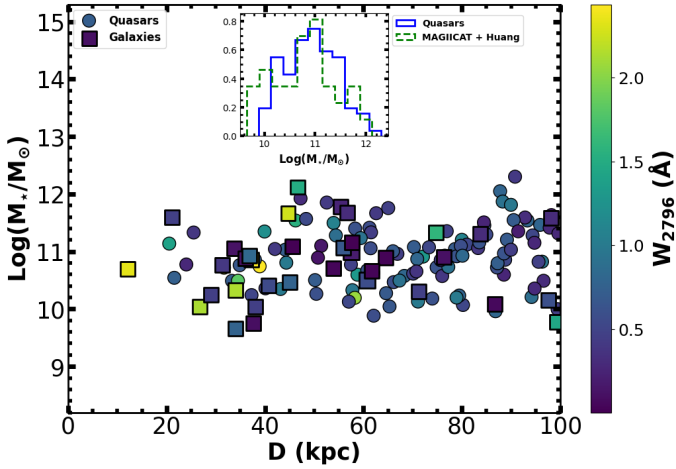


Figure 9. The plot illustrates the variation of stellar mass with the impact parameter, color-coded by the equivalent width of the detected Mg II absorption line. For quasar host galaxies the stellar mass is calculated using the relation given by Decarli et al. (2010), as given in equation 2.

sample reside in host galaxies that are not significantly more massive than the general galaxy population. Therefore, we can conclude that the similarity of the dependence of f_c and W_{2796} on D for both the samples is not influenced by a possible difference in the stellar mass distribution.

3.4 Line of sight velocity difference

Johnson et al. (2015) indicated that the velocity off-set between the systemic redshift of the quasar and Mg II absorption redshift have large spread compared to what has been found between galaxies and Mg II absorption. We have already noticed that in our redshift and stellar mass matched samples apart from a small off-set the distribution is not statistically distinguishable between galaxies and quasar host galaxies. Here we explore a possible correlation between the bolometric luminosity and line of sight velocity difference in our quasar sample. In Figure 10, we present the velocity offset between the foreground quasar redshift and its bolometric luminosity. Our analysis reveals no significant correlation between these two quantities (Spearman Rank Correlation: -0.009 , $p_{null} : 0.963$). Thus, within our sample, we find no clear evidence that the gas kinematics along the line of sight is influenced by the bolometric luminosity of quasars.

4 DISCUSSION AND CONCLUSION

It is now well established that the circumgalactic medium (CGM) consisting of metal enriched diffuse gas is a crucial component of a galaxy. The CGM serves as a reservoir of gas that regulates star formation and accretion processes. The properties of CGM are probed either through absorption lines detected in the spectra of background quasars or through the detection of diffuse emission. What is the influence of the central AGN on the properties of CGM? This is an important question to address (see Farina et al. 2014; Johnson et al. 2015; Chen et al. 2023, for using Mg II absorption as a tool). These studies have indicated that rest equivalent width of Mg II absorption and its detection rate (or covering fraction) tend to be higher around AGN host galaxies compared to the normal galaxies. It is also well

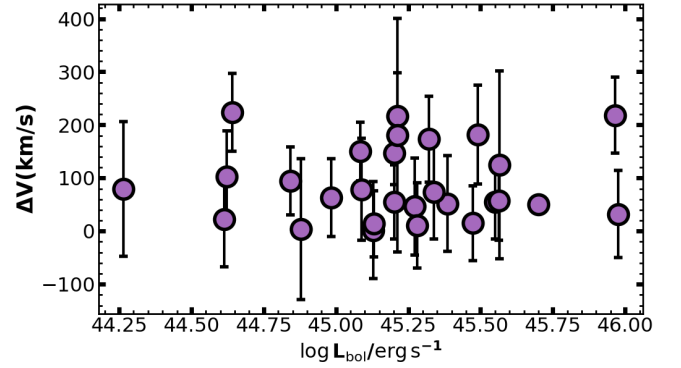


Figure 10. The figure presents the absolute velocity difference between the foreground quasar redshift and the absorber redshift as a function of the bolometric luminosity of the foreground quasar.

documented that the correlation between W_{2796} and impact parameter has a large scatter and may depend on host galaxy properties such as (i) stellar mass, (ii) luminosity and (iii) redshift etc. Therefore, it is important to probe the influence of quasars using samples that are well matched in various properties of galaxies and impact parameter distribution. This forms the main motivation of this work.

Here, we have utilized a sample of well selected 166 closely spaced quasar pairs, to probe the CGM of quasar hosting galaxies in comparison to the sample of the CGM of normal galaxies in redshift range of $0.4 \leq z \leq 0.8$ and impact parameter range of 20-100 kpc (section 2). Based on the typical SNR achieved in the SDSS spectra we mainly focus on systems having $W_{2796} \geq 1 \text{ \AA}$. As described in Section 2, our comparison galaxy sample is an amalgamation of MAGICAT (Nielsen et al. 2013) and Huang et al. (2021) sample, matching both in redshift as well as in D . Our main result is that both W_{2796} versus impact parameter (D) distribution and covering fraction (f_c) versus D distribution are statistically similar among the normal galaxies and quasar host galaxies in the aforementioned redshift and impact parameter ranges. We ensured that our results are not biased by the different impact parameter distribution of the two samples. In addition, the stellar mass distributions used for the galaxy sample and quasar host sample are statically similar (e.g., Figure 9), precluding any bias due to stellar mass dependence.

Our results are inconsistent with those of Johnson et al. (2015), who have reported enhanced W_{2796} and f_c for luminous quasar host galaxies compared to low-luminosity quasars and inactive galaxies. We note that quasars in our sample typically probe the low bolometric luminosity end of the quasar sample studied by Johnson et al. (2015). Also their sample probes a much wider redshift range. When we split our sample into two bolometric luminosity bins we do see a weak dependence of f_c on luminosity, however no correlation was present between the bolometric luminosity and W_{2796} . Moreover to confirm the strong trend in f_c with L_{bol} we need to include sample of high luminosity quasars over the same redshift range to our sample. This will alleviate the redshift evolution effects influencing the result. It is also important to extend our analysis to lower rest equivalent width limits to see whether the discrepancy is related to us mainly focusing on $W_{2796} \geq 1 \text{ \AA}$ absorbers. This can be done by freshly obtaining higher SNR spectra of quasars in our sample.

Similarly, the study by Chen et al. (2023), used large sample over full redshift range probed by SDSS to stack the background spectrum at foreground quasar redshift and showed that the W_{2796} is relatively higher in comparison to W_{2796} from CGM of normal galaxies. It will be important to revisit their analysis with a redshift and impact pa-

parameter matched samples of quasar host galaxies and normal galaxies in a restricted redshift range. Chen et al. (2023) have also noticed that detection probability of Mg II absorption along the line of sight is less than that along the transverse direction. We confirm this result in our analysis as well. Interestingly, in the case of normal galaxies the values of W_{2796} as well as f_c is found to increase with decreasing impact parameter (see for example, Guha et al. 2024). Therefore we expect both the quantities to be higher along the foreground quasar line of sight compared to what we find for higher impact parameters. In addition, one expects contribution of associated Mg II absorption also to be present along the line of sight. Therefore, less detection of Mg II absorption along the line of sight may be related to anisotropy either in the radiation field or matter distribution in the case of quasar host galaxies (see for example, Jalan et al. 2019). Therefore, our finding of similarity in the CGM properties over the impact parameter range 20-100 kpc is intriguing. As mentioned before, we do not have very many lines of sight with impact parameter < 50 kpc. It will be important to construct such a sample to confirm the presence of anisotropy in the case of quasars.

Johnson et al. (2015) have also reported an increase in the velocity off-set between the quasar host galaxy and absorption redshift with bolometric luminosity. This was also considered as one of the indications of influence of the quasar on the CGM. However, we do not find the scatter in the velocity offset values to increase with increasing luminosity of quasar host galaxies (e.g., see Figure 8). As mentioned before, it could be due to the limited bolometric luminosity range probed by our sample.

To conclude, our detailed analysis based on a sample of 166 quasars in comparison with a redshift and impact parameter matched control sample of normal galaxies, show no significant difference in the $W_{2796}-D$ and f_c-D distributions among them, indicating that low-luminosity quasars (i.e., mostly $L_{bol} \leq 10^{45}$ erg s $^{-1}$) do not substantially alter the CGM properties of the host galaxies. For further improvement, future studies should aim to observe sight-lines probing CGM of galaxies hosting luminous quasars, preferably at high SNR (for detecting low W_{2796}) and resolution (for probing kinematics), to investigate their CGM at wide range of redshift, luminosity and impact parameters (including $D < 50$ kpc as well) by carrying out controlled analysis similar to our study here.

5 ACKNOWLEDGEMENTS

The research of P.S. is supported by the University Grants Commission (UGC), Government of India, under the UGC-JRF scheme (Ref. No.: 221610014755). H.C. and P.S. express their gratitude to the Inter-University Centre for Astronomy and Astrophysics (IUCAA) for their hospitality and the provision of High-Performance Computing (HPC) facilities under the IUCAA Associate Programme. We also thank Sowgat Muzahid and Sayak Dutta for their valuable discussions during this project. Additionally, we acknowledge the assistance of AI tools, specifically OpenAI's ChatGPT, for aiding in writing and code development, and Grammarly for enhancing the text's clarity and correctness.

DATA AVAILABILITY

The data used in this study are publicly available in the DESI-EDR, and SDSS DR16 Data Release.

REFERENCES

- Abdurro'uf et al., 2022, *ApJS*, 259, 35
- Arrigoni Battaia F., Prochaska J. X., Hennawi J. F., Obreja A., Buck T., Cantalupo S., Dutton A. A., Macciò A. V., 2018, *MNRAS*, 473, 3907
- Bahcall J. N., 1978, *Phys. Scr.*, 17, 229
- Bahcall J. N., Salpeter E. E., 1966, *ApJ*, 144, 847
- Bahcall J. N., Spitzer Jr. L., 1969, *ApJ*, 156, L63
- Bergeron J., Boissé P., 1991, *A&A*, 243, 344
- Bergeron J., Stasińska G., 1986, *A&A*, 169, 1
- Borisova E., et al., 2016, *ApJ*, 831, 39
- Bowen D. V., et al., 2006, *ApJ*, 645, L105
- Burbidge E. M., 1967, *ARA&A*, 5, 399
- Burbidge E. M., Lynds C. R., Burbidge G. R., 1966, *ApJ*, 144, 447
- Burbidge G., O'Dell S. L., Roberts D. H., Smith H. E., 1977, *ApJ*, 218, 33
- Burchett J. N., Rubin K. H. R., Prochaska J. X., Coil A. L., Vaught R. R., Hennawi J. F., 2021, *ApJ*, 909, 151
- Cai Z., et al., 2019, *ApJS*, 245, 23
- Cantalupo S., Arrigoni-Battaia F., Prochaska J. X., Hennawi J. F., Madau P., 2014, *Nature*, 506, 63
- Chen H.-W., Helsby J. E., Gauthier J.-R., Shectman S. A., Thompson I. B., Tinker J. L., 2010, *ApJ*, 714, 1521
- Chen Z.-F., Qin H.-C., Cai J.-T., Zhou Y.-T., Chen Z.-G., Pang T.-T., Wang Z.-W., Cheng K.-F., 2023, *ApJS*, 265, 46
- Churchill C. W., Mellon R. R., Charlton J. C., Jannuzi B. T., Kirhakos S., Steidel C. C., Schneider D. P., 2000, *ApJ*, 543, 577
- DESI Collaboration et al., 2024, *AJ*, 168, 58
- Decarli R., Falomo R., Treves A., Labita M., Kotilainen J. K., Scarpa R., 2010, *MNRAS*, 402, 2453
- Drake A. B., Farina E. P., Neeleman M., Walter F., Venemans B., Banados E., Mazzuchelli C., Decarli R., 2019, *ApJ*, 881, 131
- Dutta R., et al., 2020, *MNRAS*, 499, 5022
- Dutta R., et al., 2021, *MNRAS*, 508, 4573
- Dutta R., et al., 2023, *MNRAS*, 522, 535
- Farina E. P., Falomo R., Scarpa R., Decarli R., Treves A., Kotilainen J. K., 2014, *MNRAS*, 441, 886
- Farina E. P., et al., 2017, *ApJ*, 848, 78
- Fossati M., et al., 2021, *MNRAS*, 503, 3044
- Fumagalli M., 2024, *arXiv e-prints*, p. arXiv:2409.00174
- Ginolfi M., Maiolino R., Carniani S., Arrigoni Battaia F., Cantalupo S., Schneider R., 2018, *MNRAS*, 476, 2421
- Guha L. K., Srianand R., 2023, *MNRAS*, 519, 3319
- Guha L. K., Srianand R., 2024, *MNRAS*, 532, 3056
- Guha L. K., Srianand R., Dutta R., Joshi R., Noterdaeme P., Petitjean P., 2022, *MNRAS*, 513, 3836
- Guha L. K., Srianand R., Petitjean P., 2024, *MNRAS*, 527, 5075
- Gunn J. E., Peterson B. A., 1965, *ApJ*, 142, 1633
- Guo Y., et al., 2020, *ApJ*, 898, 26
- Hennawi J. F., Prochaska J. X., 2013, *ApJ*, 766, 58
- Hewett P. C., Wild V., 2010, *MNRAS*, 405, 2302
- Huang Y.-H., Chen H.-W., Shectman S. A., Johnson S. D., Zahedy F. S., Helsby J. E., Gauthier J.-R., Thompson I. B., 2021, *MNRAS*, 502, 4743
- Jalan P., Chand H., Srianand R., 2019, *ApJ*, 884, 151
- Johnson S. D., Chen H.-W., Mulchaey J. S., 2015, *MNRAS*, 452, 2553
- Joshi R., Das S., Fumagalli M., Fossati M., Péroux C., Chaudhary R., Yesuf H. M., Ho L. C., 2024, *arXiv e-prints*, p. arXiv:2412.07835
- Krogager J.-K., 2018, *arXiv e-prints*, p. arXiv:1803.01187
- Lan T.-W., 2020, *ApJ*, 897, 97
- Lyke B. W., et al., 2020, *ApJS*, 250, 8
- Martin D. C., Chang D., Matuszewski M., Morrissey P., Rahman S., Moore A., Steidel C. C., 2014, *ApJ*, 786, 106
- Mishra S., Chand H., Krishna G., Joshi R., Shchekinov Y. A., Fatkhullin T. A., 2018, *MNRAS*, 473, 5154
- Nielsen N. M., Churchill C. W., Kacprzak G. G., Murphy M. T., 2013, *ApJ*, 776, 114
- O'Sullivan D. B., Martin C., Matuszewski M., Hoadley K., Hamden E., Neill J. D., Lin Z., Parihar P., 2020, *ApJ*, 894, 3
- Opher R., 1974, *Nature*, 250, 310

- Petitjean P., Bergeron J., 1990, *A&A*, **231**, 309
Roeser H. J., 1975, *A&A*, **45**, 329
Sandage A., 1965, *ApJ*, **141**, 1560
Sargent W. L. W., Young P., Schneider D. P., 1982, *ApJ*, **256**, 374
Srianand R., Khare P., 1994, *ApJ*, **428**, 82
Steidel C. C., Sargent W. L. W., 1992, *ApJS*, **80**, 1
Tumlinson J., Peebles M. S., Werk J. K., 2017, *ARA&A*, **55**, 389
Wu Q., Shen Y., 2022, *ApJS*, **263**, 42

This paper has been typeset from a $\text{\TeX}/\text{\LaTeX}$ file prepared by the author.